Progress In Electromagnetics Research C, Vol. 173, 152–157, 2026

PIER C

(Received 3 May 2026, Accepted 8 June 2026, Scheduled 5 September 2026)

Dielectric and Anomalous Dispersion Behavior of Conductive Polyaniline Carbon Nanotube Composite at X-Band Frequencies

Puthanpurakkal S. Sreekala* and Selvaraj Gokul

Department of Electronics, PSG College of Arts and Science, Coimbatore, near civil aerodrome, Tamil Nadu 641014, India

ABSTRACT: This paper provides a detailed discussion of anomalous dispersion studies of polyaniline carbon nanotube composites (PANI-CNT) in the X-band frequency range. Dielectric properties are used to demonstrate the material's anomalous behavior. Measurement analysis is performed using a network analyzer; the anomalous medium shows a phase advance, while the other shows a gradual phase decrease. By correlating these characteristics, we can observe their significant impact on the material's microwave properties. We present PANI-CNT powder throughout the study. PANI-CNT exhibits enormous microwave enhancement characteristics compared to standard materials. This paper examines various microwave parameters, including permittivity and shielding efficiency. The novelty of the anomalous effect lies in the significant enhancement of shielding efficiency it produces.

1. INTRODUCTION

Conducting polymer-based nanocomposites have attracted significant attention due to their tunable electrical, dielectric, and electromagnetic properties, which make them suitable for microwave absorption, electromagnetic interference (EMI) shielding, and high-frequency electronic applications [1–3]. Among conducting polymers, polyaniline (PANI) has been widely investigated owing to its ease of synthesis, environmental stability, controllable electrical conductivity through protonic doping, and low cost [1, 2]. However, pristine PANI exhibits limited dielectric loss and moderate conductivity at microwave frequencies, restricting its effectiveness in high-frequency applications. To overcome these limitations, carbon-based nanofillers such as carbon nanotubes (CNTs) have been incorporated into the PANI matrix. CNTs possess exceptional electrical conductivity, high aspect ratio, and strong interfacial interaction with polymers, leading to the formation of conductive pathways even at low filler concentrations [3, 4]. The resulting PANI-CNT composites exhibit enhanced charge transport, interfacial polarization, and dielectric loss, which are essential for effective microwave attenuation, particularly in the X-band frequency range (8–12 GHz) used in radar and satellite communication systems.

The dielectric behavior of polymer nanocomposites at microwave frequencies is governed by multiple polarization mechanisms, including electronic, dipolar, and interfacial (Maxwell-Wagner-Sillars) polarization [5]. At higher frequencies, some of these polarization processes fail to follow the alternating electric field, resulting in frequency-dependent permittivity and dielectric loss [6]. In conductive polymer composites, this often leads to anomalous dispersion, in which the dielectric constant and loss factor exhibit non-monotonic or reversed frequency dependence rather than the conventional decreasing trend with frequency [6, 7]. In PANI-CNT composites, anomalous dispersion behavior at X-band frequencies is strongly influenced by CNT loading, dispersion quality, and interfacial coupling between the polymer chains and nanotubes. The presence of CNTs introduces additional relaxation processes and hopping conduction mechanisms, which enhance dielectric loss through conduction loss and polarization lag [7, 8]. These effects contribute significantly to microwave absorption and EMI shielding efficiency by improving impedance matching and energy dissipation within the composite.

Therefore, understanding the dielectric response and anomalous dispersion behavior of conductive PANI-CNT composites in the X-band frequency region is crucial for optimizing their electromagnetic performance. The present study analyzes the frequency-dependent dielectric properties of PANI-CNT composites, elucidates the underlying polarization and conduction mechanisms responsible for anomalous dispersion, and highlights their potential for advanced microwave and EMI shielding applications.

2. EXPERIMENTAL SECTION

2.1. Materials

Aniline monomer ($\geq$ 99%, analytical grade) was obtained by distillation under reduced pressure before use. Ammonium peroxydisulfate (APS), hydrochloric acid (HCl, 37%), and ammonia solution (NH_4OH, 25%) were of analytical grade and used without further purification. Distilled water was used throughout the experiment.

* Corresponding author: Puthanpurakkal S. Sreekala (sreekala@psgcas.ac.in).

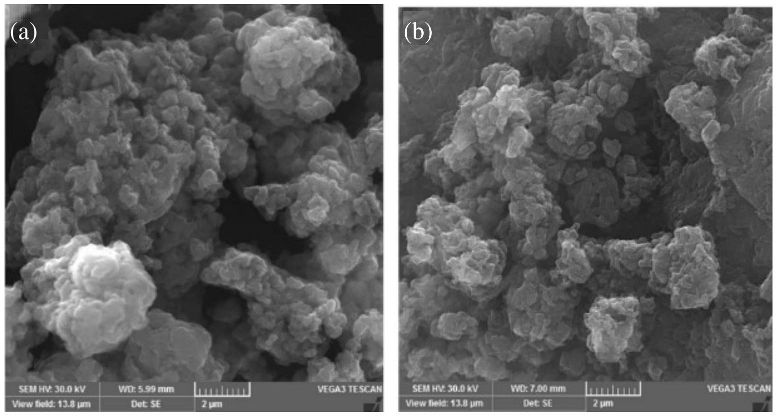

FIGURE 1. SEM images of (a) PANI and (b) PANI-CNT.

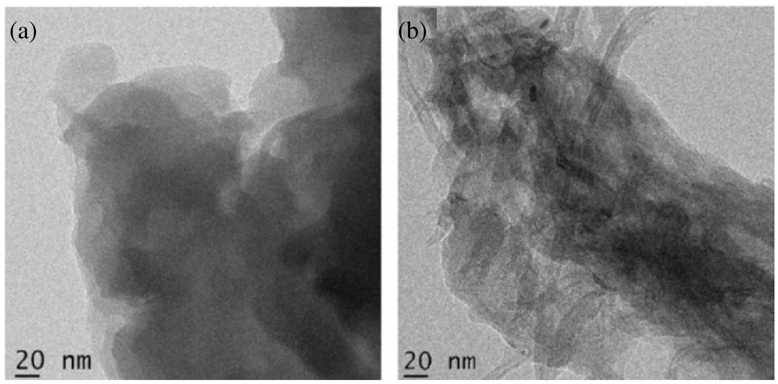

FIGURE 2. TEM images of (a) PANI and (b) PANI-CNT.

2.2. Synthesis of HCl-Doped Polyaniline (PANI)

Polyaniline (PANI) was synthesized by chemical oxidative polymerization in an acidic medium. Distilled aniline (4 mL) was dissolved in 1 M HCl under continuous stirring. An oxidant solution was prepared by dissolving 9.99 g of ammonium persulfate (APS) in 1 M HCl and added dropwise to the aniline solution under vigorous stirring. The mixture was ultrasonicated for 30 min and stirred for 12 h in an ice-water bath at 1–5°C. The resulting dark-green HCl-doped PANI precipitate was filtered and washed repeatedly with 1 M HCl followed by distilled water until the filtrate became colourless. The product was dried at 50°C to constant weight and ground into a fine powder for further use.

The dried PANI was dedoped in 0.5 M ammonia solution, filtered, washed with distilled water, and dried at 60°C for 24 h. It was then re-doped in 1 M HCl overnight, washed, and dried at 80°C. The HCl-doped PANI powder was used for X-band dielectric characterization.

2.3. Synthesis of Polyaniline-Carbon Nanotube (PANI-CNT) Composite by In Situ Single-Phase Polymerization

An in situ polymerization method was used to synthesize the PANI-CNT composite. CNTs (0.6 g) were dispersed in 100 mL of 1 M HCl by ultrasonication for 30 min, followed by the addition of 4.65 g aniline and further sonication for 30 min. An APS solution in 1 M HCl was added dropwise, and the reaction was stirred for 12 h at 0–5°C. The resulting PANI-CNT composite was filtered, washed with distilled water and acetone, and dried at 60°C for 24 h.

The composite was dedoped in 0.5 M NH_4OH, washed to neutral pH, and dried at 80°C for 48 h. It was then re-doped in 1 M HCl for 24 h, filtered, washed with distilled water, and dried at 60°C. The obtained HCl-doped PANI-CNT composite was used for microwave and material characterization.

3. RESULTS AND DISCUSSION

3.1. Morphology: SEM and TEM

The surface and internal morphologies of pristine polyaniline (PANI) and the PANI-carbon nanotube (PANI-CNT) composite were examined by scanning electron microscopy (SEM) and transmission electron microscopy (TEM), as shown in Fig. 1 and Fig. 2, respectively. The SEM image of pristine PANI (Fig. 1(a)) exhibits a granular, highly agglomerated cauliflower-like morphology with limited interparticle connectivity. In contrast, the PANI-CNT composite (Fig. 1(b)) shows a more interconnected structure, where CNTs bridge adjacent PANI grains, reducing agglomeration and improving structural continuity.

The TEM image of pristine PANI (Fig. 2(a)) reveals densely packed polymer domains with limited long-range

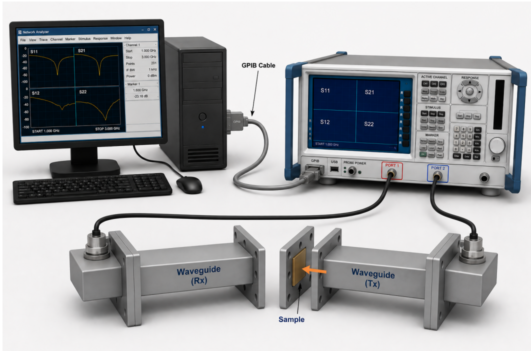

FIGURE 3. Waveguide measurement setup.

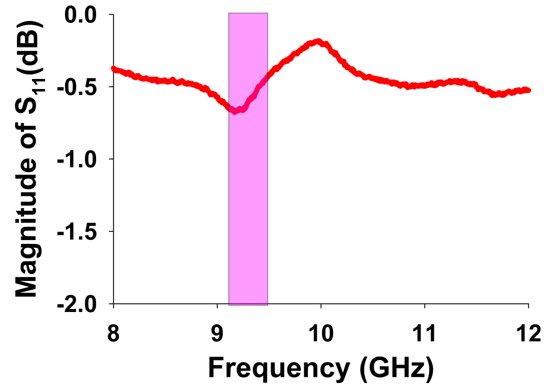

FIGURE 4. Magnitude of reflection coefficient (S_{11}).

ordering, restricting charge transport and interfacial polarization. Conversely, the TEM image of the PANI-CNT composite (Fig. 2(b)) confirms the uniform dispersion of CNTs coated with PANI, forming a conductive network with a large interfacial area. This hierarchical structure enhances Maxwell-Wagner-Sillars interfacial polarization and charge transport, leading to the improved dielectric constant and dielectric loss observed in the X-band frequency range.

Figure 3 shows the schematic representation of the waveguide measurement setup. The specimen with 1.53 mm thickness was fabricated with dimensions matching the internal cross-section of the rectangular waveguide. It was inserted into the waveguide sample holder between two flanged waveguide sections, which were securely fastened using screws. This ensured that the specimen completely filled the waveguide aperture with negligible air gaps, thereby minimizing lateral electromagnetic leakage and maintaining field confinement within the waveguide during S-parameter measurements. A 1.53 mm thick specimen was inserted into the waveguide, and calibrated reflection and transmission coefficients (S_{11} and S_{21}) were measured over the operating frequency range. The complex relative permittivity was extracted from the calibrated S-parameters using the Nicholson-Ross-Weir (NRW) method by determining the propagation constant and wave impedance. The analysis accounts for the specimen thickness, waveguide cutoff frequency, and dominant-mode propagation, providing accurate characterization of electromagnetic properties.

3.2. Microwave Characterization

The reflection coefficient (S_{11}) of the PANI-CNT composite remains close to 0 dB across the X-band frequency range, with only a shallow minimum observed near ~9.5–10 GHz (Fig. 4). The measured S_{11} exhibits frequency-dependent minima influenced by both the finite thickness of the composite specimen and the material's frequency-dependent dielectric properties. Since interference effects can produce similar S_{11} variations even in non-dispersive dielectric slabs, the anomalous dispersion is identified from the extracted complex permittivity (ε' and ε'') rather than from the S_{11} response alone. The S_{11} data are therefore interpreted as supporting evidence of the dielectric behavior of the PANI-CNT composite. This behavior can be directly interpreted as anomalous dielectric dispersion arising from the composite's frequency-dependent complex permittivity. In materials exhibiting anomalous dispersion, the real (ε') part of the permittivity varies non-monotonically with frequency due to competing polarization and conduction mechanisms. In the present PANI-CNT system, interfacial polarization and hopping conduction dominate the dielectric response at microwave frequencies, which modify both the real (ε') and imaginary (ε'') components of the complex permittivity. These changes alter the composite's effective input impedance. Since the magnetic permeability remains close to unity ($\mu_r \approx 1$), the impedance cannot be matched to free space (377 Ω) over a broad frequency range. Consequently, a significant portion of the incident electromagnetic wave is reflected despite enhanced dielectric loss. The frequency-dependent complex permittivity influences the S_{11} response of the PANI-CNT composite by modifying its effective input impedance. The anomalous dispersion of ε' causes impedance mismatch with free space, resulting in high reflection across the X-band, while the shallow minimum near 9.7 GHz indicates improved impedance matching due to the combined effect of ε' and ε''. Although specimen thickness and multiple internal reflections also affect S_{11}, its frequency dependence is consistent with the observed anomalous dielectric dispersion.

The measured transmission coefficient ($|S_{21}|$) of Fig. 5 exhibits a deep minimum near 9.6–9.8 GHz (≈ -50 dB), coinciding with the anomalous dispersion region. At this frequency, the maximum ε'' and steep decrease in ε' indicate strong di-

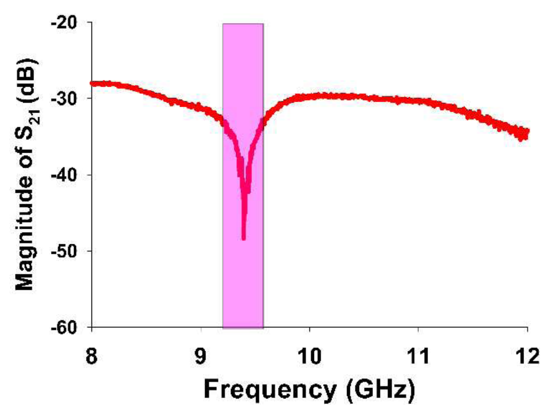

FIGURE 5. Magnitude of transmission coefficient (S_{21}).

electric loss and resonance-controlled polarization, leading to enhanced energy dissipation through interfacial polarization, charge-carrier hopping, and conduction loss in the CNT network. Together with multiple internal reflections, these mechanisms suppress microwave transmission and confirm the dominant role of anomalous dielectric dispersion in the EMI shielding performance of the PANI-CNT composite.

Figure 6 presents the reflection (R), transmission (T), and absorption (A) characteristics of the PANI-CNT composite in the X-band (8–12 GHz). The reflection coefficient ($R = |S_{11}|^2$) remains high (0.75–0.90), indicating significant impedance mismatch with free space and strong surface reflection. The transmission coefficient ($T = |S_{21}|^2$) is nearly zero throughout the band, confirming negligible microwave transmission due to high dielectric loss and multiple internal reflections. The absorption coefficient ($A = 1 - R - T$) varies between 0.10 and 0.25, with a maximum near 9–10 GHz, where enhanced dielectric loss associated with anomalous dispersion increases electromagnetic energy dissipation. Overall, the high reflection, negligible transmission, and moderate absorption demonstrate that the composite acts as an effective EMI shielding material by suppressing microwave propagation through the combined effects of impedance mismatch, dielectric loss, and internal reflections.

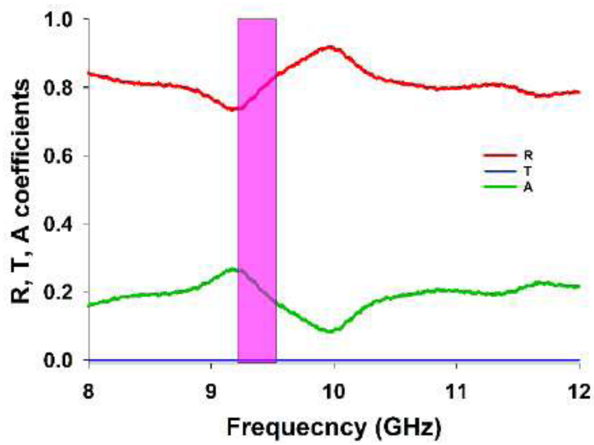

FIGURE 6. Reflection (R), transmission (T), and absorbance (A) coefficients of the PANI-CNT sample.

The frequency dependence of the real part of permittivity (Fig. 7) in the range 8–12 GHz exhibits pronounced anomalous dispersion behavior, characterized by sharp variations and sign reversals in specific frequency bands. A prominent peak followed by a steep decline is observed near 9.3 GHz, where the real part of permittivity rapidly decreases with increasing frequency. This behavior is a clear signature of anomalous dispersion, which typically occurs near a strong electromagnetic resonance. In this region, the permittivity also attains negative values, indicating a resonance-induced plasmonic or metamaterial-like response.

A second anomalous dispersion region is evident near 11 GHz, where another abrupt drop in the real part of permittivity is observed, followed by gradual recovery at higher frequencies. These rapid variations confirm the existence

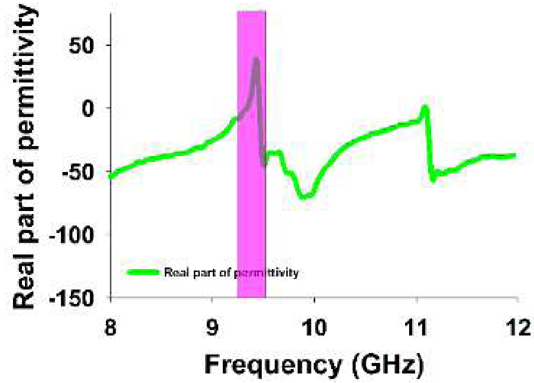

FIGURE 7. Real part of the permittivity of PANI-CNT.

of multiple resonant modes within the operating frequency band. Physically, anomalous dispersion arises due to strong coupling between the incident electromagnetic wave and the oscillating bound charges in the material. Near the resonance frequency, enhanced energy absorption occurs, leading to a peak in the imaginary part of permittivity and a corresponding steep decrease in its real part, as required by the Kramers-Kronig relations. The observed negative permittivity in anomalous dispersion regions further confirms the dominance of resonance-driven electric polarization, which is consistent with the Lorentz oscillator model. Therefore, the measured permittivity response clearly demonstrates that the material exhibits strong resonance-controlled anomalous dispersion behavior in the microwave frequency range.

The imaginary part of the complex permittivity (ε'') shows a pronounced loss peak (Fig. 8) around 9.2–9.5 GHz, indicating enhanced dielectric loss due to anomalous dispersion. This behavior arises from interfacial polarization, charge carrier hopping, and dipolar relaxation in the PANI-CNT composite, resulting in efficient conversion of electromagnetic energy into heat. Beyond this frequency, ε'' decreases, indicating reduced dielectric loss. The enhanced dielectric loss in the anomalous dispersion region contributes significantly to the attenuation of transmitted microwaves (lower S_{21}) in the X-band.

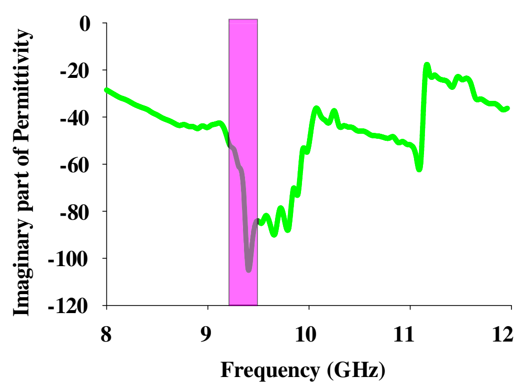

FIGURE 8. Imaginary part of the permittivity of PANI-CNT.

In Fig. 9, the phase is "unwrapped" to remove discontinuities at $\pm 180°$, yielding a continuous curve. The curve generally decreases, but exhibits regions where the slope changes.

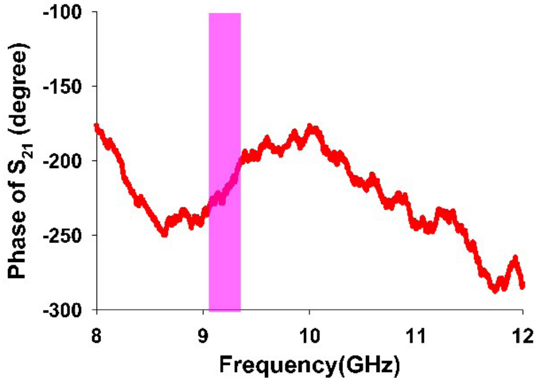

FIGURE 9. Phase of S_{21} of the PANI-CNT sample.

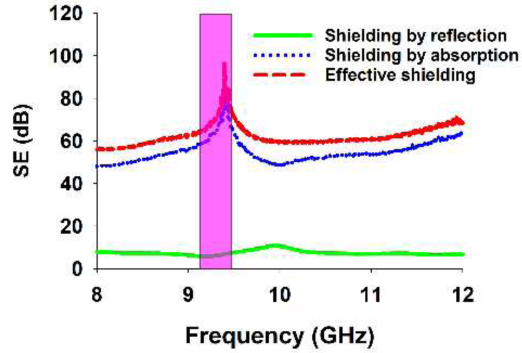

FIGURE 10. Shielding Efficiency (SE).

This presents a phase-based investigation of anomalous dispersion characteristics of a microwave structure, using the unwrapped phase of the transmission coefficient (S_{21}) over the frequency range 8–12 GHz. The measured phase response exhibits regions of rapid slope variation and phase reversal, clear indicators of anomalous dispersion. The observed phase nonlinearity is attributed to strong resonance effects and reactive energy storage within the structure. The phase response confirms the presence of fast-wave and backward-wave propagation regions, without the need for group-delay extraction. The unwrapped S_{21} phase decreases overall with increasing frequency, indicating forward-wave propagation. However, the phase curve exhibits three distinct regions: a low-frequency region from 8 GHz to 9 GHz. This region shows a smooth, monotonic phase decrease, indicating normal dispersion. There is a mid-frequency region that spans from 9.5 to 10.3 GHz. This part of the phase slope becomes weak and partially reverses, which indicates anomalous dispersion. The high-end frequency region spans 10.5–12 GHz. In this region, the phase slope becomes steep again and returns to normal dispersive behavior. Anomalous dispersion is confirmed in the mid-frequency band by phase slope reduction and compression, local phase curvature reversal, and strong nonlinearity in the phase profile. These effects indicate that the electromagnetic energy undergoes resonant redistribution. Such phase-controlled anomalous dispersion is essential for compact phase shifters, CRLH transmission lines, resonant waveguides, RF metamaterial circuits, and pulse shaping networks.

The frequency-dependent shielding effectiveness (SE) of the structure in the 8–12 GHz (Fig. 10) range exhibits a pronounced resonance-enhanced response, and the total effective shielding (SE_T) reaches a maximum of approximately 95 dB near 9.5 GHz. The shielding contribution is primarily dominated by absorption (SE_A), while the reflection component (SE_R) remains comparatively small across the entire frequency band. This behavior clearly indicates that the shielding mechanism is absorption-controlled rather than reflection-dominated. The sharp enhancement in both SE_A and SE_T near 9.5 GHz directly corresponds to the material's anomalous dispersion region. In dispersive electromagnetic media, anomalous dispersion occurs when the frequency derivative of the real part of permittivity becomes negative, ($d\varepsilon'/d\omega < 0$), which is necessarily accompanied by a strong peak in the imaginary part of permittivity due to Kramers-Kronig relations. This simultaneous rapid variation of real permittivity and enhanced dielectric loss is the fundamental physical origin of the observed shielding enhancement. Near the resonance frequency, strong coupling between the incident electromagnetic wave and the resonant dipolar oscillations within the structure leads to a substantial increase in dielectric loss. As a result, the electromagnetic energy is efficiently dissipated within the material rather than reflected, leading to a dominant absorption-shielding component. The Lorentz-type resonance responsible for this anomalous dispersion produces intense polarization currents that convert the incident electromagnetic energy into heat through ohmic and dielectric losses, thereby maximizing SE_A. The relatively low and slowly varying reflection shielding across the band further confirms effective impedance matching between free space and the structure near resonance. When anomalous dispersion drives the real part of permittivity toward values that improve impedance matching, surface reflection is minimized, and more energy enters the material, where it is subsequently absorbed. This mechanism explains why the effective shielding (SE_T) closely follows the absorption shielding profile. Therefore, the sharp peak in total shielding effectiveness near 9.5 GHz is a direct consequence of resonance-induced anomalous dispersion, where the rapid dispersive variation of permittivity and enhanced dielectric loss work synergistically to produce exceptionally high absorption-dominated electromagnetic interference shielding performance in the microwave frequency range.

4. CONCLUSION

In this paper, the electromagnetic response of the proposed structure has been investigated in terms of permittivity dispersion, transmission characteristics, and shielding effectiveness in the 8–12 GHz microwave frequency band. The real part of the permittivity exhibits clear resonance-induced anomalous dispersion, including rapid spectral variations and negative permittivity regions near the resonance frequencies. These features confirm that the structure's electromagnetic behavior is governed by Lorentz-type electric resonances, consistent with classical dispersion theory. The transmission response further validates this behavior, where a deep attenuation in the $|S_{21}|$ spectrum coincides with the anomalous dispersion region, indicating strong suppression of electromagnetic wave propagation. Furthermore, the shielding analysis reveals exceptionally high total shielding effectiveness near resonance, predominantly governed by absorption rather than reflection. This absorption-dominated shielding is attributed to enhanced dielectric losses associated with strong resonant polarization.

The strong correlation among anomalous dispersion, transmission suppression, and enhanced absorption-driven shielding confirms the effectiveness of the proposed structure for practical microwave applications such as EMI shielding, absorbers, and filter devices.

ACKNOWLEDGEMENT

The authors gratefully acknowledge the financial support provided by the Institutional Research Seed Grant (IRSG 2024-2025) of PSG College of Arts and Science, which enabled the successful completion of this research work.

REFERENCES

[1] Wang, J., Q. Sun, J. Li, Y. Guo, W. Tian, Y. Liu, B. Wu, L. Deng, N. Mahmood, and X. Jian, "Polymer-based nanocomposites: Role of interface for effective microwave absorption," *Materials Today Physics*, Vol. 31, 100981, 2023.

[2] Kausar, A. and I. Ahmad, "Conducting polymer nanocomposites for electromagnetic interference shielding — Radical developments," *Journal of Composites Science*, Vol. 7, No. 6, 240, 2023.

[3] Omana, L., A. Chandran, R. E. John, R. Wilson, K. C. George, N. V. Unnikrishnan, S. S. Varghese, G. George, S. M. Simon, and I. Paul, "Recent advances in polymer nanocomposites for electromagnetic interference shielding: A review," *ACS Omega*, Vol. 7, No. 30, 25 921–25 947, 2022.

[4] Byrne, M. T. and Y. K. Gun'ko, "Recent advances in research on carbon nanotube-polymer composites," *Advanced Materials*, Vol. 22, No. 15, 1672–1688, 2010.

[5] Dang, Z.-M., J.-K. Yuan, J.-W. Zha, T. Zhou, S.-T. Li, and G.-H. Hu, "Fundamentals, processes and applications of high-permittivity polymer-matrix composites," *Progress in Materials Science*, Vol. 57, No. 4, 660–723, 2012.

[6] Chen, J., Z. Pei, B. Chai, P. Jiang, L. Ma, L. Zhu, and X. Huang, "Engineering the dielectric constants of polymers: From molecular to mesoscopic scales," *Advanced Materials*, Vol. 36, No. 52, 2308670, 2024.

[7] Yang, M., M. Guo, E. Xu, W. Ren, D. Wang, S. Li, S. Zhang, C.-W. Nan, and Y. Shen, "Polymer nanocomposite dielectrics for capacitive energy storage," *Nature Nanotechnology*, Vol. 19, No. 5, 588–603, 2024.

[8] Chen, M., J. Zhu, K. Zhang, H. Zhou, Y. Gao, J. Fan, R. Chen, and H.-L. Wang, "Carbon nanofiber/polyaniline composite aerogel with excellent electromagnetic interference shielding, low thermal conductivity, and extremely low heat release," *Nano-Micro Letters*, Vol. 17, No. 1, 80, 2025.